Electronic Supplementary Material (ESI) for Nanoscale.
This journal is © The Royal Society of Chemistry 2021

Magnetic and Dielectric Property Control in the Multivalent Nanoscale Perovskite $Eu_{0.5}Ba_{0.5}TiO_3$

Nasim Farahmand[a,b,c], Christine K. McGinn[d], Qize Zhang[b,c,e], Zheng Gai[f], Ioannis Kymissis[d] and Stephen O'Brien[a,b,c*]

Supplementary Information (S.I.)

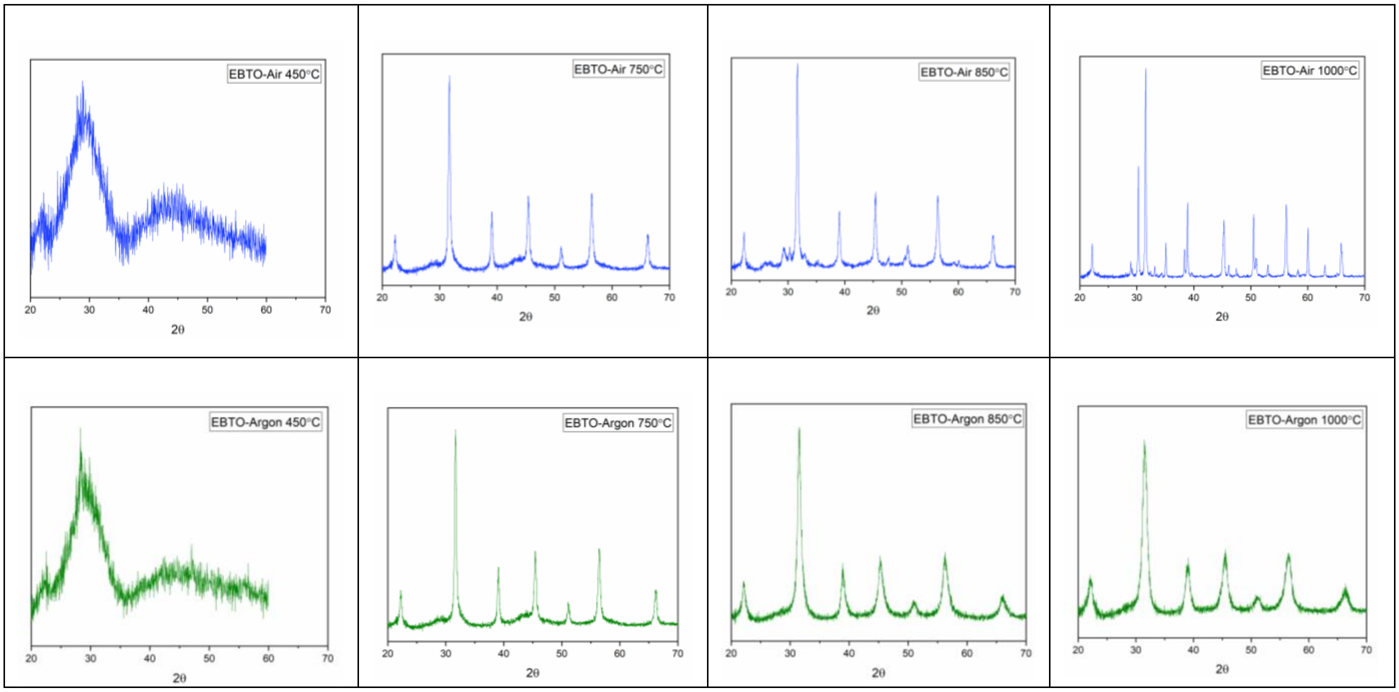

Figure S1. X-ray diffraction of both samples (air in blue, argon in green) at 450°C, 750°C, 850°C and 1000°C.

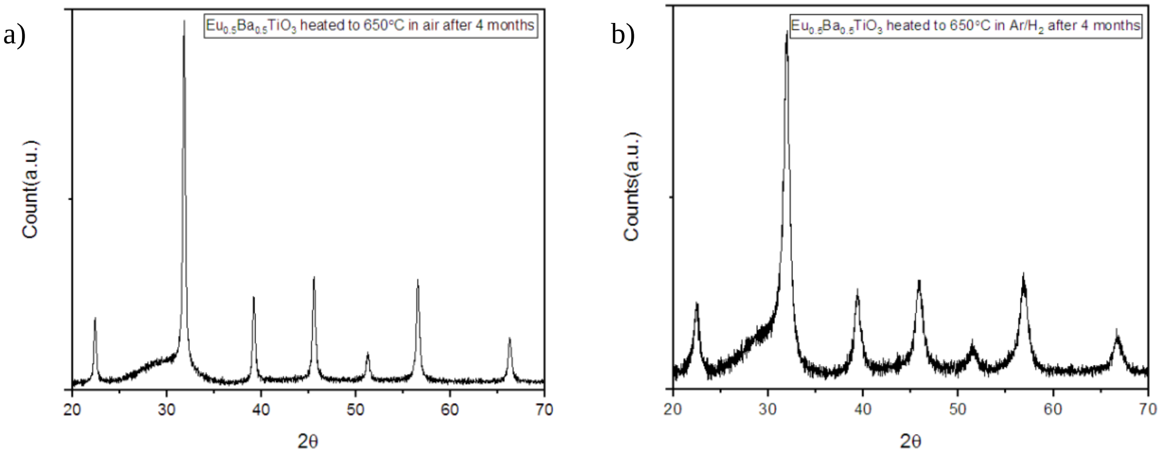

Figure S2. X-ray diffraction of EBTO-Air(a) and EBTO-Argon(b), showing the perovskite structure after 4 months exposure to air/moisture. The shoulder to the left of the (110) peak is attributed to carbonate formation at the surface the nanoparticles.

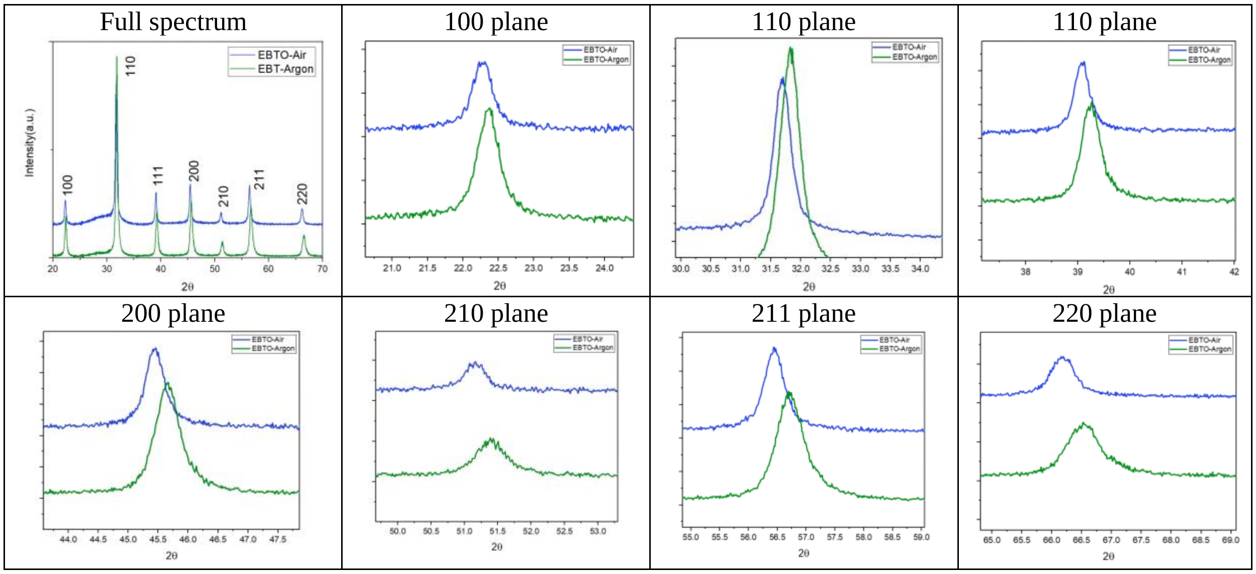

Figure S3. XRD spectrum and magnified selected peak positions for EBTO-Air(blue) and EBTO-Argon(green) heated to 650 °C

a)

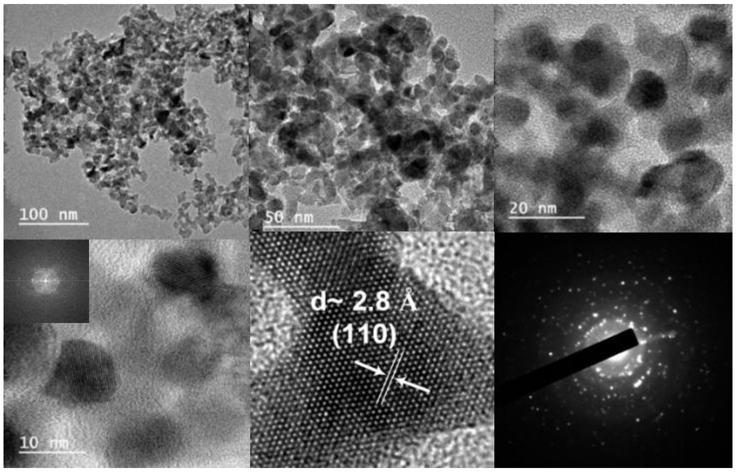

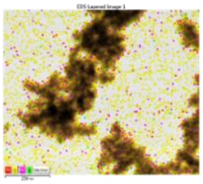

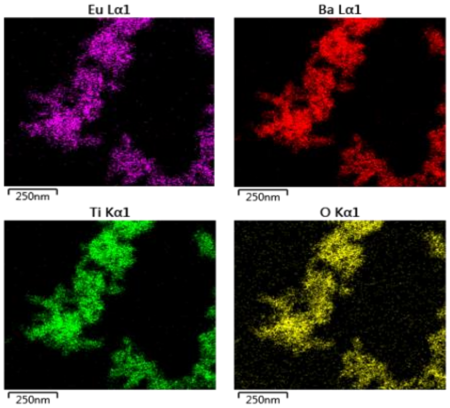

Element	Atomic Wt%
Eu	6.29
Ba	6.83
Ti	17.41
O	74.47

b)

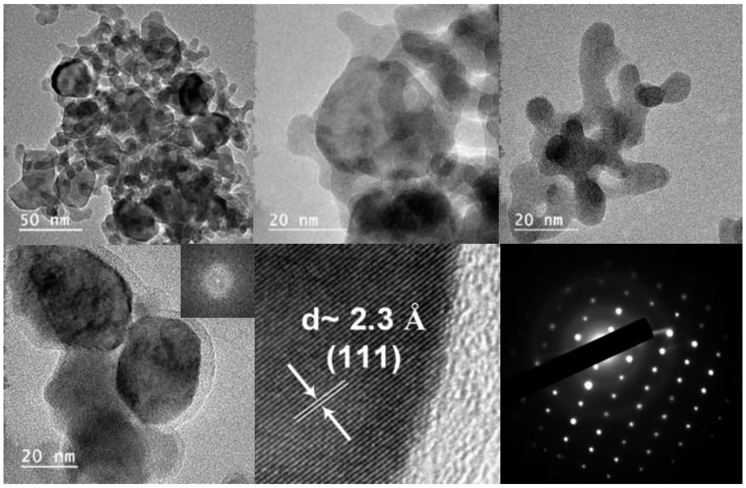

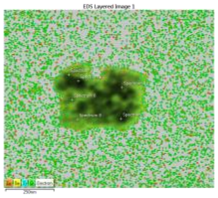

Element	Atomic%
Eu	7.95
Ba	10.46
Ti	15.68
O	65.90

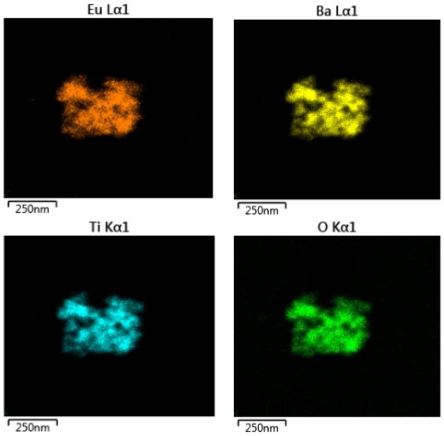

(c)

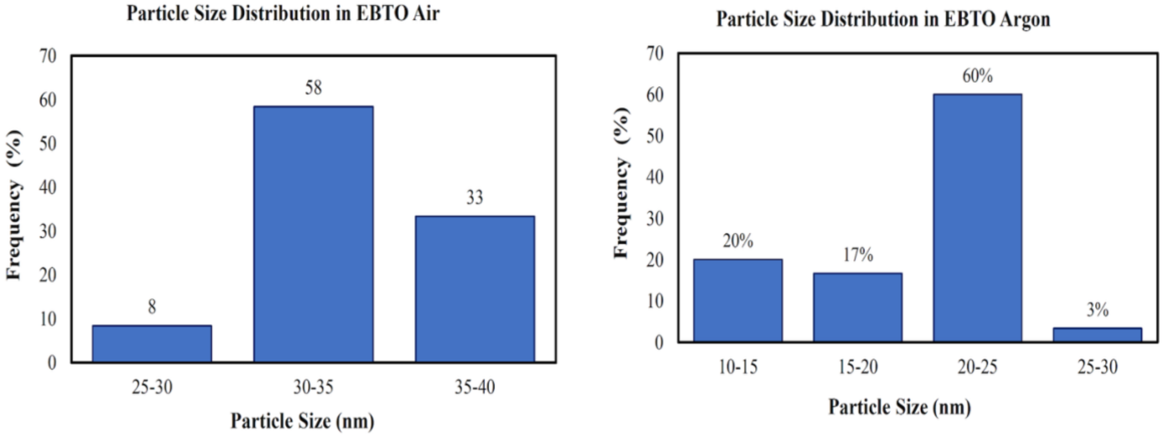

Figure S4. a) TEM images and EDS mapping of EBTO-Argon (particle size: 10-20 nm), b) TEM images and EDS mapping of EBTO-Air (particle size: 30-40 nm), (c) Particle size distribution analysis of the two samples.

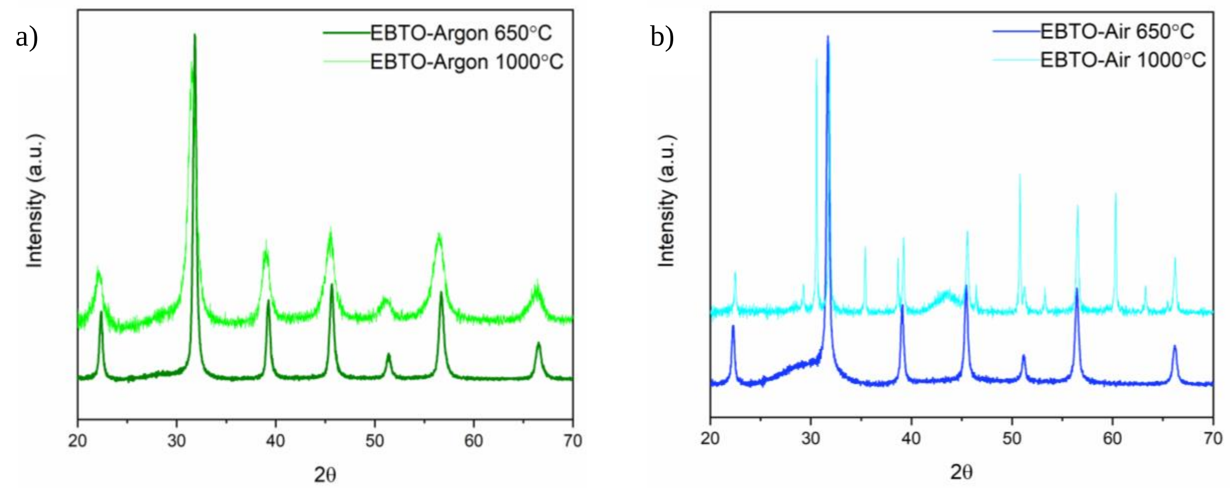

Figure S5. XRD of EBTO-Argon (a) and EBTO-Air (b). The darker color in each graph indicates heating to 650°C and the lighter color indicates heating to 1000°C

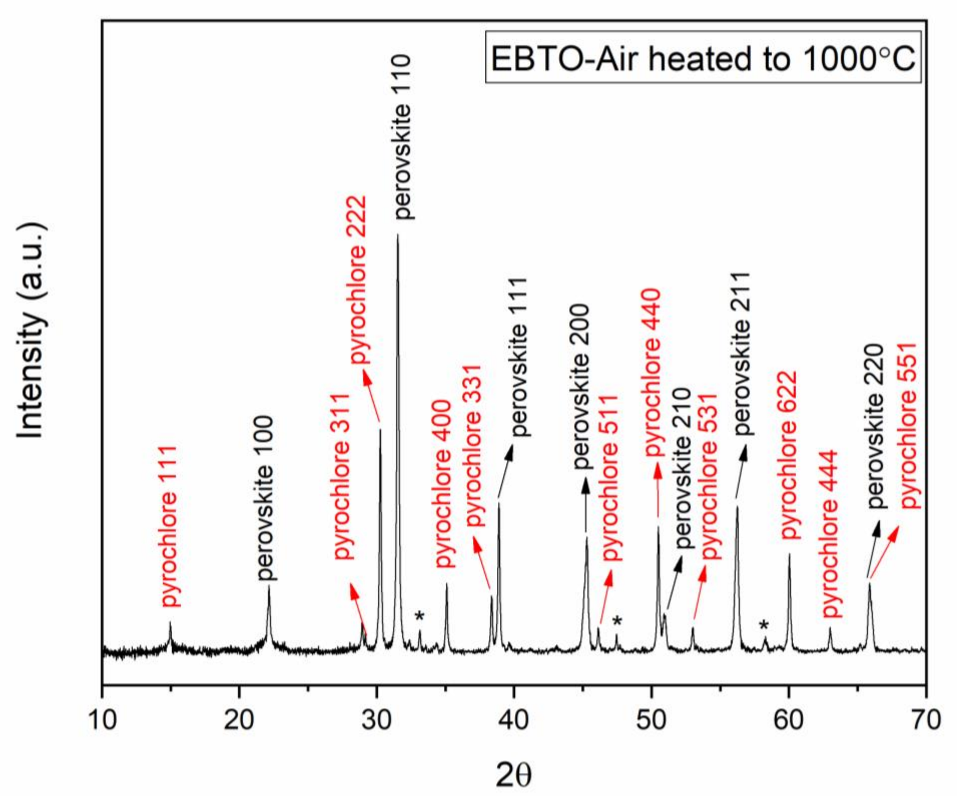

Figure S6. Labelled XRD of EBTO-Air heated to 1000° C. The peaks attributed to perovskite are shown in black, while the pyrochlore peaks are in red. There are three more peaks in positions around 33°, 47° and 58° 2θ attributed to Eu_2O_3.[1,2,3]

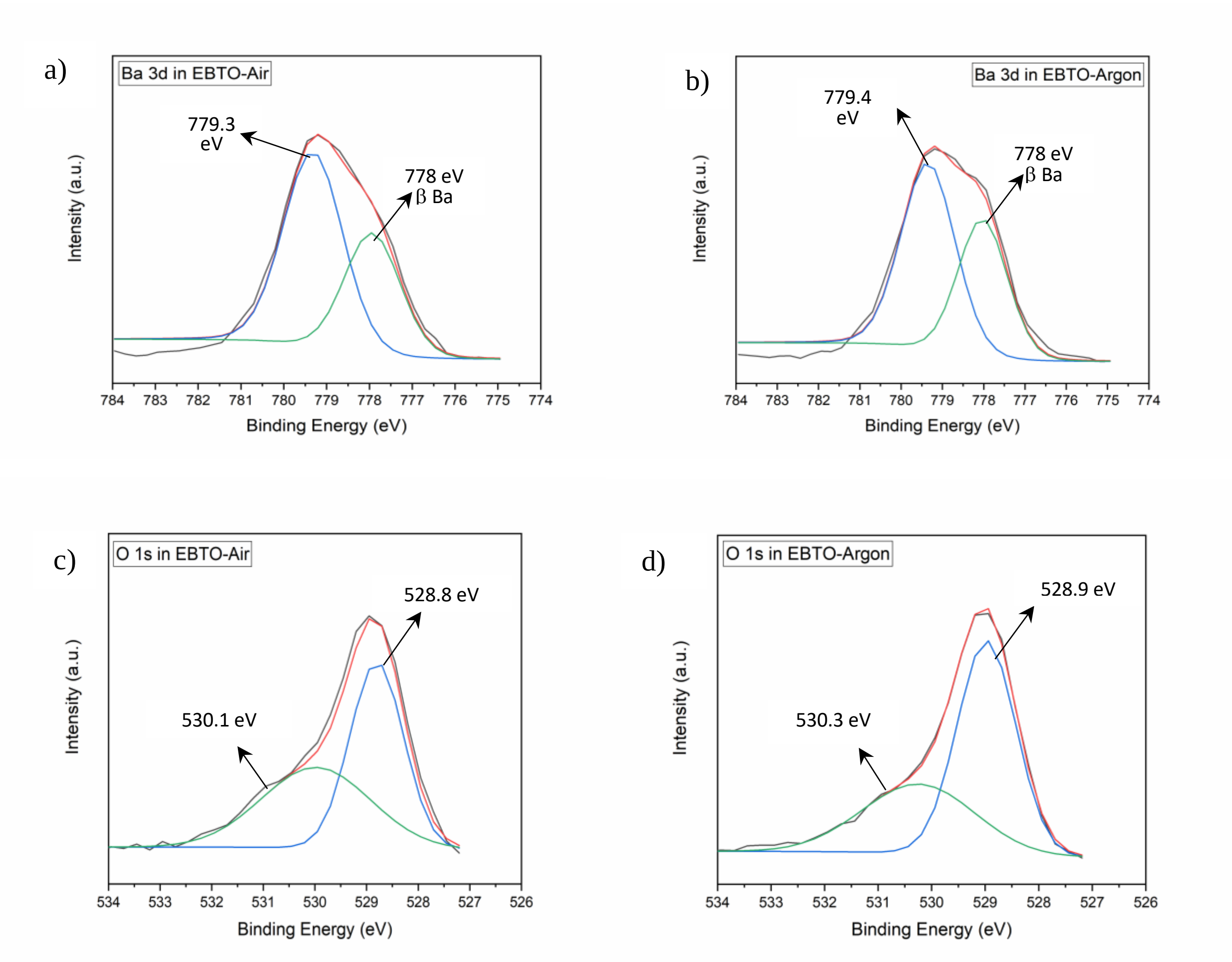

Figure S7. XPS spectra of Barium 3d (a and b) and Oxygen 1s (c and d) in EBTO-Air and EBTO-Argon

Figure S8. Europium in EtOH, followed by gel formation (top), the gel readily oxidizes in air transforming from black to white (bottom)

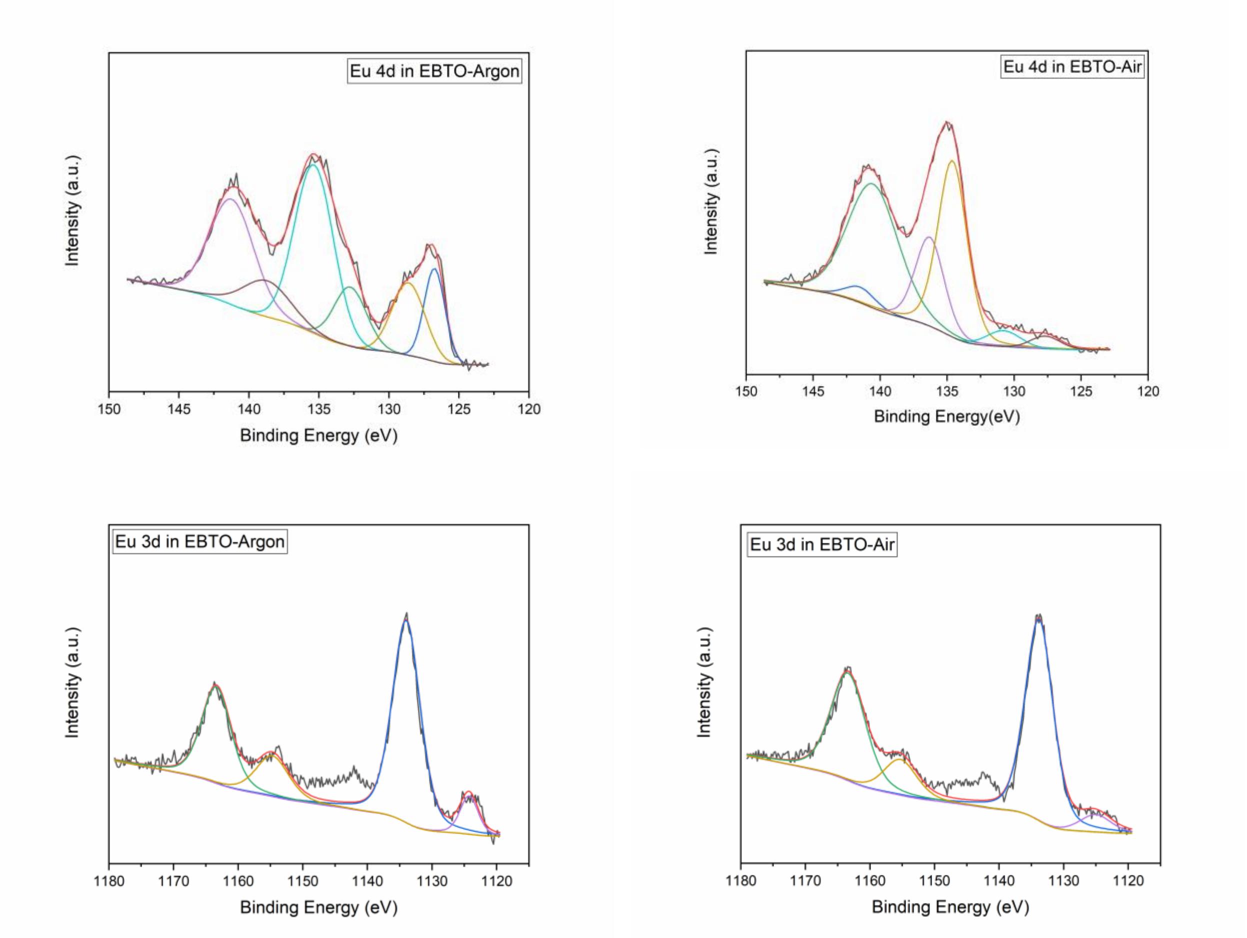

Figure S9. XPS of Eu 3d and Eu 4d spectra without background subtraction in EBTO-Air and EBTO-Argon samples.

The XPS spectra for the 4d peak shows a striking difference between the two samples. For the binding energy region 125.5-145.5 eV, peaks can be observed. These peaks are due attributed to photoelectron collection from the 4d shell of the europium atoms, be they in the Eu(II) or Eu(III) oxidation state. Previously reported XPS studies indicate that up to five peaks can be observed for Eu 4d binding energies, generally assigned as Eu^{2+} $4d_{3/2}$(~130-132 eV and ~135 eV)[4–6], Eu^{3+} $4d_{5/2}$(~137 eV), Eu^{3+} $4d_{3/2}$(~141 eV)[4,6]. Our observed data is consistent with these previous observations with the exception of the peak centered around 135eV which is two convoluted peaks.

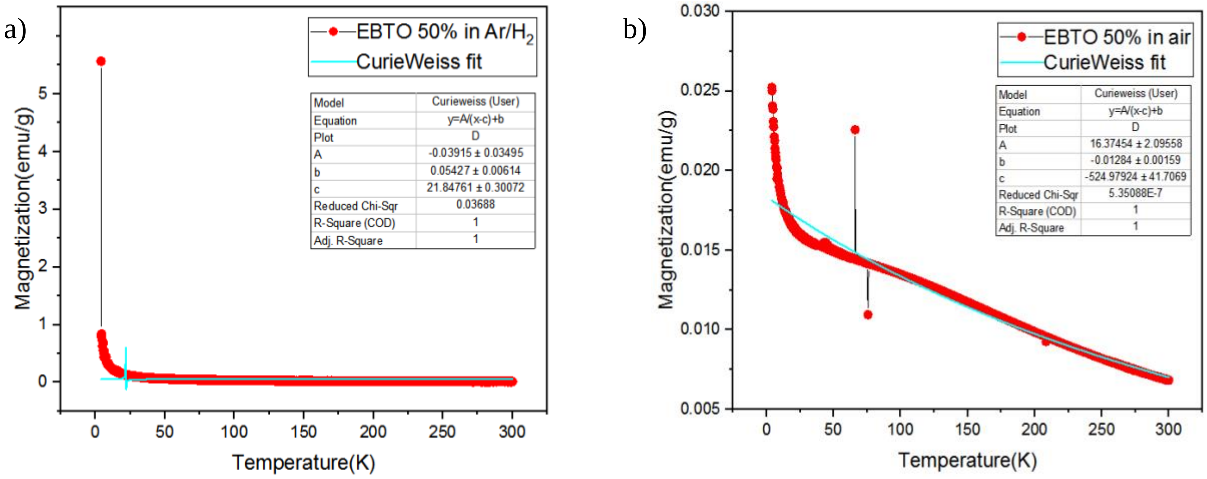

Model	Curieweiss (User)
Equation	y=A/(x-c)+b
Plot	D
A	-0.03915 ± 0.03495
b	0.05427 ± 0.00614
c	21.84761 ± 0.30072
Reduced Chi-Sqr	0.03688
R-Square (COD)	1
Adj. R-Square	1

Model	Curieweiss (User)
Equation	y=A/(x-c)+b
Plot	D
A	16.37454 ± 2.09558
b	-0.01284 ± 0.00159
c	-524.97924 ± 41.7069
Reduced Chi-Sqr	5.35088E-7
R-Square (COD)	1
Adj. R-Square	1

Figure S10. M-T curves for EBTO-Argon(a) and EBTO-Air(b)

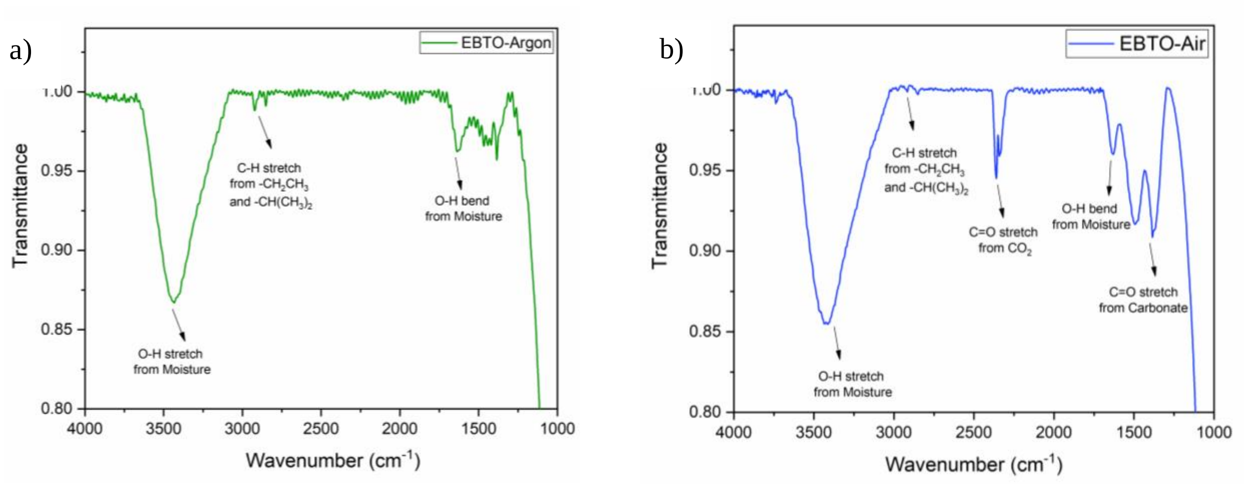

Figure S11. FTIR of EBTO-Argon(a) and EBTO-Air(b) left under ambient conditions. EBTO-Air is observed to absorb CO_2 from the atmosphere with the formation of $BaCO_3$ (especially ~ months), which can be removed by washing with H_2O or H^+/H_2O.

Goldschmidt tolerance factor calculation

$$t = \frac{r_A + r_O}{\sqrt{2}(r_B + r_O)}$$

r_A: radius of cation A

r_B: radius of cation B
r_O: radius of Oxygen (anion)

	Ba^{2+}	Eu	Ti	O^{2-}
Coordination number	12	9 (Eu^{2+}), 9 (Eu^{3+})	6	2
Shannon ionic radii	161 pm	130 pm, 112 pm	67 pm (Ti^{3+}), 61 pm (Ti^{4+})	135 pm

for $BaTiO_3$:

$$t = \frac{r_A + r_O}{\sqrt{2}(r_B + r_O)} = \frac{161 + 135}{\sqrt{2}(61 + 135)} = 1.06$$

for $EuTiO_3$:

$$t = \frac{r_A + r_O}{\sqrt{2}(r_B + r_O)} = \frac{130 + 135}{\sqrt{2}(61 + 135)} = 0.96$$

for $Ba_{0.5}Eu_{0.5}TiO_3$ for entirely Eu^{2+}:

$$t = \frac{r_A + r_O}{\sqrt{2}(r_B + r_O)} = \frac{0.5(161) + 0.5(130) + 135}{\sqrt{2}(61 + 135)} = 1.01$$

for $Ba_{0.5}Eu_{0.5}TiO_3$ with a mixture of 50% Eu^{3+}/Eu^{2+} (without Ti^{3+}/Ti^{4+} consideration):

$$t = \frac{r_A + r_O}{\sqrt{2}(r_B + r_O)} = \frac{0.5(161) + 0.25(130) + 0.25(112) + 135}{\sqrt{2}(61 + 135)} = 0.99$$

for $Ba_{0.5}Eu_{0.5}TiO_3$ with a mixture of 50% Eu^{3+}/Eu^{2+} (with Ti^{3+}/Ti^{4+} consideration):

$$t = \frac{r_A + r_O}{\sqrt{2}(r_B + r_O)} = \frac{0.5(161) + 0.25(130) + 0.25(112) + 135}{\sqrt{2}(0.5(67) + 0.5(61) + 135)} = 0.98$$

In general:

$$\begin{cases} t > 1 : \text{Hexagonal or Tetrahedral} \\ 0.9 < t < 1 : \text{Cubic} \\ 0.71 < t < 0.9 : \text{Orthorhombic/Rhombohedral} \\ t < 0.71 : \text{Different Structures} \end{cases}$$

References

(1) Zhu, Y.; Zhai, X.; Wang, L. Hydrothermal Synthesis of Ln(OH)3 Nanorods and the Conversion to Ln2O3 (Ln = Eu, Nd, Dy) Nanorods via Annealing Process. *J. Nanomater.* **2013**, *2013* (3). https://doi.org/10.1155/2013/130514.

(2) Kang, J. G.; Jung, Y.; Min, B. K.; Sohn, Y. Full Characterization of Eu(OH) 3 and Eu 2 O 3 Nanorods. *Appl. Surf. Sci.* **2014**, *314*, 158–165. https://doi.org/10.1016/j.apsusc.2014.06.165.

(3) Barad, C.; Kimmel, G.; Hayun, H.; Shamir, D.; Hirshberg, K. Phase Stability of Nanocrystalline Grains Of.

(4) Jankowska-Sumara, I.; Sitko, D.; Podgórna, M.; Pilch, M. The Electromechanical Behavior of Europium Doped BaTiO3. *J. Alloys Compd.* **2017**, *724*, 703–710. https://doi.org/10.1016/j.jallcom.2017.07.090.

(5) Sagarna, L.; Rushchanskii, K. Z.; Maegli, A.; Yoon, S.; Populoh, S.; Shkabko, A.; Pokrant, S.; Ležaić, M.; Waser, R.; Weidenkaff, A. Structure and Thermoelectric Properties of EuTi(O,N) 3 ± δ. *J. Appl. Phys.* **2013**, *114* (3). https://doi.org/10.1063/1.4813098.

(6) Kim, D.; Jin, Y. H.; Jeon, K. W.; Kim, S.; Kim, S. J.; Han, O. H.; Seo, D. K.; Park, J. C. Blue-Silica by Eu2+-Activator Occupied in Interstitial Sites. *RSC Adv.* **2015**, *5* (91), 74790–74801. https://doi.org/10.1039/c5ra15641f.